ACS APPLIED MATERIALS & INTERFACES

Research Article

www.acsami.org

Multidimensional Thin Film Hybrid Electrodes with MoS_2 Multilayer for Electrocatalytic Hydrogen Evolution Reaction

Eungjin Ahn[†] and Byeong-Su Kim*[,†,‡]

[†]Department of Energy Engineering and [‡]Department of Chemistry, Ulsan National Institute of Science and Technology (UNIST), Ulsan 44919, Korea

Supporting Information

ABSTRACT: Hybrid electrodes are widely used in various energy storage and conversion devices. However, conventional fabrication methods like simple mixing allow only limited control over the internal electrode structure, and it is often difficult to elucidate the structure−property relationship among the electrode components. Taking advantage of the versatile layer-by-layer (LbL) assembly method, herein we report the preparation of electrocatalytic thin film electrodes for hydrogen evolution reaction (HER), highlighting the importance of nanoscale composition in multidimensional hybrid electrodes. The fabrication utilized the electrostatic interaction between the two components: catalytically active two-dimensional MoS_2 nanosheets and conductive, one-dimensional multiwalled carbon nanotube (MWNT) support. The electrocatalytic activity was found to be highly tunable by adjusting the thickness of the electrode, suggesting structural dependence of electron transfer and mass transport between the electrolyte and electrode, which is otherwise difficult to investigate in electrodes fabricated by simple conventional methods. Furthermore, the detailed mechanism of HER on the hybrid electrode was also investigated, revealing the fine balance between the catalytic activity of MoS_2 and conductivity of MWNT. We anticipate that this unique approach will offer new insights into the nanoscale control of electrode architecture and the development of novel electroactive catalysts.

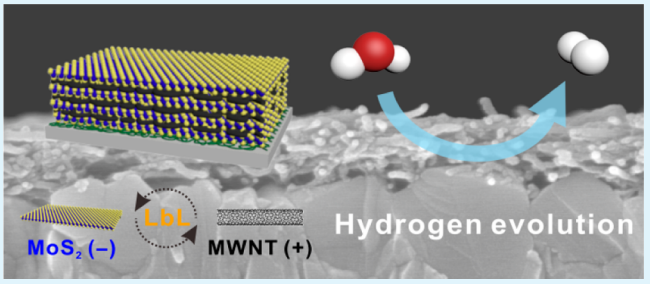

KEYWORDS: *electrocatalyst, hydrogen evolution reaction, chemically exfoliated molybdenum disulfide, multiwalled carbon nanotube, layer-by-layer assembly*

1. INTRODUCTION

The rapid depletion of fossil fuels and growing environmental concerns have created a global demand for alternative energy sources that are clean and renewable.[1] Among the many technological advances in electrochemical energy conversion, the hydrogen-based fuel cell has received considerable attention as an attractive option for next-generation energy source, owing to its high energy density and environmentally benign operation.[2,3] Hydrogen generation is generally achieved through the hydrogen evolution reaction (HER) from water. While platinum and its alloys are still the most popular electrocatalysts for HER, their natural scarcity and associated high cost have spurred the relentless pursuit of alternative catalysts with reliable electrochemical performance.

Molybdenum disulfide (MoS_2) is a promising candidate to substitute noble metal catalysts for electrochemical HER from water, due to its relatively low cost, high catalytic activity, and high stability.[4,5] In particular, the small energy variation of MoS_2 for the adsorption of proton and subsequent desorption of hydrogen during HER offers a significant opportunity for developing MoS_2-based electrocatalysts.[6−10] In order to optimize the active edge sites over the inert basal plane of MoS_2, considerable efforts have been dedicated to synthesize various MoS_2 structures with a higher number of edge sites,[2,11] including nanoparticles,[12,13] mesoporous materials,[14,15] nanowires,[16,17] and thin films.[18,19]

Among these materials, the colloidal suspension of two-dimensional (2D) MoS_2 sheets is very attractive, due to by taking advantages of their large surface areas as well facile synthetic nature of the sheets in a controllable and scalable manner. However, the suspension of chemically exfoliated MoS_2 sheets is often in the metastable 1T phase, which changes into the thermodynamically more stable semiconducting 2H phase or becomes oxidized into insulating structures. Thus, it often requires a carefully chosen conductive support as its electrocatalytic activity is known to be strongly influenced by the supporting materials. A number of approaches have been reported to address these issues, such as using graphene sheets or carbon fiber as a conductive support for MoS_2.[13,20] Perhaps the most facile approach to improve the catalytic activity of the electrode is using a simple mixture of MoS_2 and conductive carbon based support. Nevertheless, maintaining the ordered architecture and preventing severe aggregation in the electrodes are often very challenging.

Received: November 29, 2016
Accepted: February 27, 2017
Published: February 27, 2017

DOI: 10.1021/acsami.6b15251
ACS Appl. Mater. Interfaces 2017, 9, 8688−8695

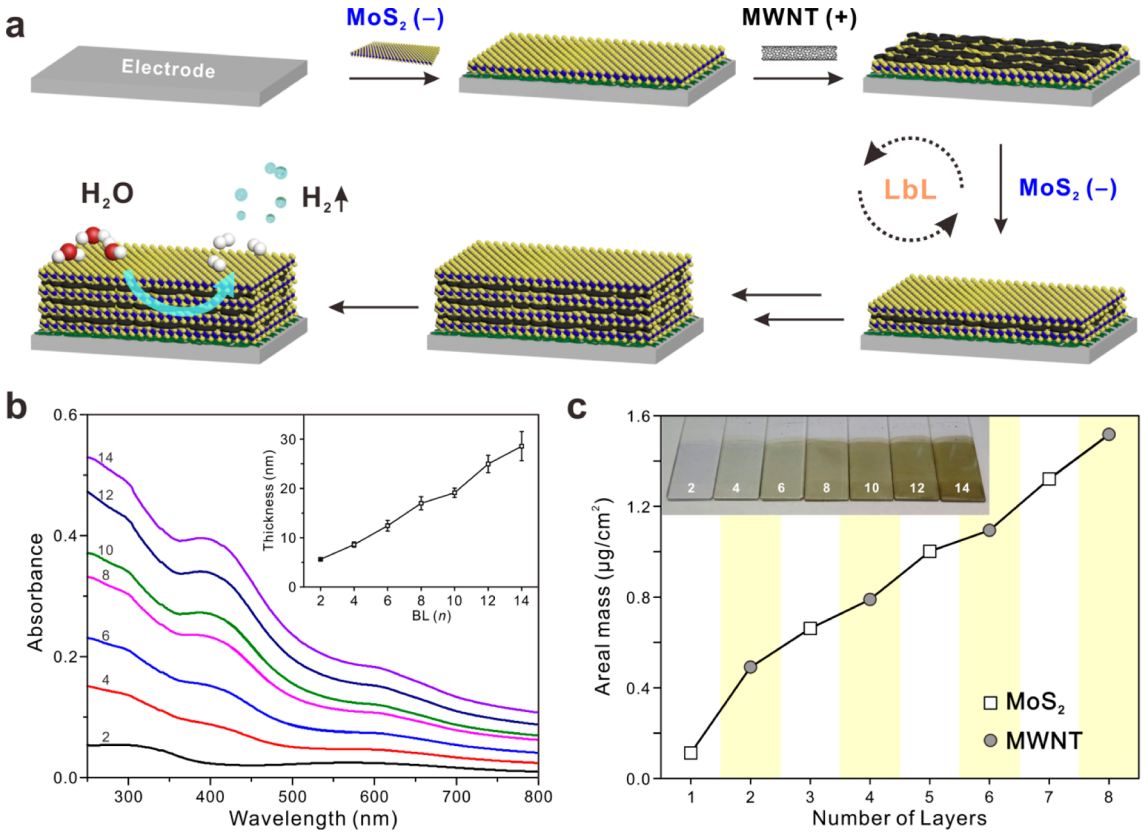

Figure 1. (a) Schematic of the LbL assembly of $(MoS_2/MWNT)_n$ multilayer electrode for HER from water. (b) UV−vis absorbance spectra, showing the growth of $(MoS_2/MWNT)_n$ multilayers. The number of bilayers (BL, n) in the film is labeled in the graph. Inset shows the linear growth of the multilayer thickness as measured by ellipsometry. (c) QCM analysis of mass loading for each cycle of MoS_2 and MWNT deposition. Inset shows the photograph of the multilayer films deposited on a quartz slide with different number of BL.

In this regard, the layer-by-layer (LbL) assembly offers many opportunities for preparing multilayer thin films for desired functions, as it is a truly nanoscale blending method with nanometer-precision control over the composition and thickness.[21−31] The integration of carbon nanostructures, such as carbon nanotubes and graphene nanosheets into multilayer films by LbL assembly has been recently demonstrated in multiple examples including our own studies.[32−39] Nevertheless, many of these studies are focused on creating electrically conducting thin-film electrodes.

Herein, we report the unique integration of electrocatalytic 2D MoS_2 nanosheets with one-dimensional (1D) carbon nanotube support by LbL assembly, to create three-dimensional (3D) structured hybrid electrocatalytic thin-film electrodes that are active toward HER. Specifically, the negatively charged MoS_2 sheets in suspension and the positively charged multiwalled carbon nanotubes (MWNT) are assembled through their electrostatic interactions on a silicon wafer or fluorine-doped tin oxide (FTO) coated glass slide, which results in the hybrid multilayer thin films of MoS_2 supported by carbon nanotubes. In this study, the MWNT not only serves as a structural component within the multilayer films but also as a catalytic support layer due to its high conductivity and unique 1D morphology that can create porosity within the 3D hybrid electrodes, thereby ensuring high mass transfer rates in the electrochemical system. Although there are several reports on MoS_2[40−43] or hybridized MoS_2-MWNT based electrocatalyst[44,45] with noticeable catalytic performances toward HER, to the best of our knowledge, this is the first report of conventional LbL-assembled electrocatalytic thin film for hydrogen evolution catalysis. We find that the versatile LbL assembly method allows the integration of materials of varying dimensions into hybrid electrocatalytic thin films in a highly controllable manner. In particular, the catalytic performance strongly depends on the thickness of the electrode (i.e., the number of bilayers (BL)). We also explore the mechanism of electrocatalytic HER behavior on the thermally treated hybrid electrode, as the treatment strongly influences the phase of the MoS_2 nanosheets and the conductivity of the MWNT within the multilayer.

2. RESULTS AND DISCUSSION

Bulk MoS_2 powder was exfoliated into a suspension of MoS_2 sheets using a well-established lithium intercalation method, which generates negative charges on the surface of MoS_2 sheets due to the adsorption of OH^- ions.[46] After extensive cycles of purification, the as-prepared MoS_2 suspension displayed fairly good colloidal stability without noticeable aggregation for several months. According to the atomic force microscopy (AFM) measurements, the majority of the exfoliated MoS_2 sheets were around a few hundred nanometers in width and 2.0−2.6 nm in thickness. The thickness indicates that the exfoliated MoS_2 nanosheets are tri- and tetra-layers, compared to that of fully exfoliated MoS_2 monolayers (0.60−0.70 nm; see Figure S1 in the Supporting Information for details).

Meanwhile, a stable dispersion of chemically modified MWNT was prepared based on our previous report.[47] The typical oxidation in strong acids introduced carboxylic acid

DOI: 10.1021/acsami.6b15251
ACS Appl. Mater. Interfaces 2017, 9, 8688−8695

groups onto the surface of the MWNT. The carboxylic acid groups further reacted with excess ethylenediamine through the reaction mediated by *N*-ethyl-*N*-(3-(dimethylamino)propyl) carbodiimide (EDC) methiodide to afford the positively charged MWNT with free amine groups (MWNT-NH_2). FT-IR results confirmed the presence of the reactive surface functional groups in MWNT-NH_2 (Figure S2). Specifically, a broad peak at 3440 cm^{-1} and a strong peak at 1631 cm^{-1} can be ascribed to NH stretching in amine and C═O stretching, respectively, due to the formation of the amide linkage.[48,49] According to the zeta-potential measurement, both negatively charged MoS_2 and positively charged MWNT suspensions possessed sufficient colloidal stability with zeta potentials of −38.3 ± 0.8 mV for MoS_2 and +41.1 ± 1.7 mV for MWNT-NH_2 at pH 5 (LbL assembly condition; Figure S3).

With these two stable suspensions carrying opposite charges, their electrostatic interaction was exploited to assemble the hybrid multilayer electrodes on a silicon wafer or FTO-coated glass slide, by repeated alternating deposition of the two suspensions, resulting in a multilayered architecture of $(MoS_2/MWNT)_n$ with the typical number of bilayers (BL, n = 2−14). The experimental procedures are schematically shown in Figure 1a and detailed in the Supporting Information. It should be noted that a polyaniline (PANi) primer layer was first coated in order to increase the initial adhesion to the substrate for effective film growth.

The successful buildup of the multilayer was confirmed by UV−vis spectroscopy, ellipsometry, and quartz crystal microbalance (QCM) analysis (Figure 1b,c). The gradually increased absorbance at the characteristic peaks at 250 nm for MWNT and 395 nm for MoS_2 indicates an increasing number of layers, demonstrating the linear growth of the hybrid $(MoS_2/MWNT)_n$ multilayer electrode. As reported in our previous study of MoS_2 multilayer spaced by polyelectrolyte layers, the as-assembled film did not exhibit the characteristic excitonic peaks of MoS_2 without thermal treatment, suggesting the presence of the metastable 1T-form of MoS_2 sheets synthesized by Li-intercalation and exfoliation method.[38] In accordance with the absorbance spectra, ellipsometry measurements showed that the thickness of the multilayer increased linearly with increasing number of BLs, with an average BL thickness of 1.77 ± 0.06 nm. The QCM analysis results further supported the linear growth of the $(MoS_2/MWNT)_n$ multilayers. The average mass of each component within a single BL was determined to be 0.20 $\mu g/cm^2$ for MoS_2 and 0.14 $\mu g/cm^2$ for MWNT, resulting in a mass density ratio of between MoS_2 and MWNT approximately to 1.5:1 within a single BL. This result is critical for building a comparable control set consisting of a simple mixture of MoS_2 and MWNT, in order to highlight the importance of nanoscale architecture in the electrode through LbL assembly for high electrocatalytic performance.

After confirming the successful growth of $(MoS_2/MWNT)_n$ films, we assembled the multilayers on FTO-glass substrates (Figure S4) prior to performing the electrochemical analysis. As a control, the two solutions were mixed and drop-casted using the mass ratio determined from QCM analysis. SEM surface morphology showed a clear difference between the LbL-assembled multilayers and drop-casted mixture of MoS_2 and MWNT (Figure 2). The former showed a relatively smooth morphology with a regular porous structure, compared to that of the drop-casted control. Therefore, the LbL assembly technique is important for the nanoscale blending of two heterogeneous components into a controlled architecture. In

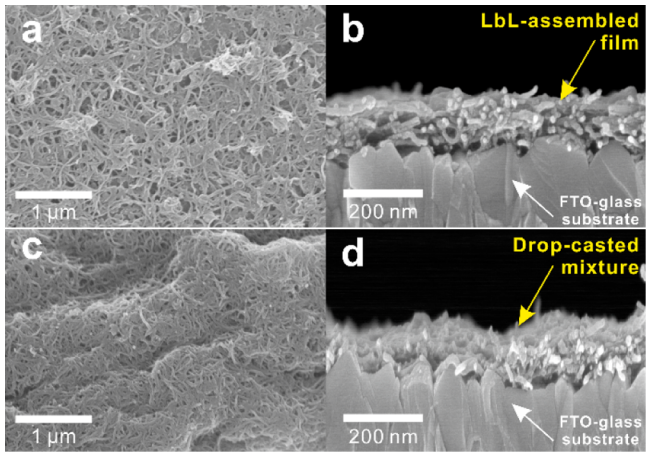

Figure 2. SEM images of (a, b) LbL-assembled $(MoS_2/MWNT)_{14}$ film and (c, d) drop-casted MoS_2-MWNT mixture. The substrate is FTO-coated glass (see Figure S4 for photographs of the films).

the cross-section view, the thicknesses of the LbL-assembled and drop-casted samples were both measured as ∼150 nm. The difference between this value and that obtained from ellipsometry could be originated from difference of intrinsic surface roughness between the FTO-coated glass and the silicon wafer.

To further confirm the presence of MoS_2 and MWNT in the multilayer film, Raman analysis was performed (Figure S5). Raman spectroscopy is the most direct and nondestructive technique to characterize the structures of various nanomaterials. The characteristic Raman peaks indicated the E^1_{2g} (381.4 cm^{-1}) and A_{1g} (405.5 cm^{-1}) vibration modes of MoS_2. In addition, the peak separation between them (∼24 cm^{-1}) also supported the presence of MoS_2 nanosheets with three to four layers, in accord with the AFM observation. Three characteristic peaks of MWNT were observed: the D-band (1351 cm^{-1}), G-band (1588 cm^{-1}), and 2D-band (2692 cm^{-1}).[50] The strong D-band of MWNT was attributed to the damaged graphitic structures via introduction of amine moiety onto the nanotube surface.

The catalytic activity for HER was evaluated by electrochemical analysis in 0.50 M H_2SO_4 electrolyte using a three-electrode system with the assembled $(MoS_2/MWNT)_n$ film on FTO-coated glass substrate, Pt foil, and saturated calomel electrode (SCE) being the working, counter, and reference electrodes, respectively (inset in Figure 3a). The simple mixture of MoS_2 and MWNT with no structural control was employed for comparison as described earlier. As shown in Figure 3, the current density increased linearly with the thickness of the $(MoS_2/MWNT)_n$ multilayer electrode. This is not surprising, as more catalytic sites and conductive supporting material deposited on the electrode would enhance the electrochemical activity. Interestingly, however, this trend changed when BL is over 14, where the current density decreased with increasing film thickness. The origin of this phenomenon will be the subject of our discussion as follows: For HER electrocatalysts, the relationship between the overpotential (η) and the current density (J) is described by the cathodic term of the Butler−Volmer equation, known as the Tafel eq 1:

$$J = J_0 \times 10^{\eta/b} \quad (1)$$

,where J is the measured current density, J_0 is the exchange current density, and η is the overpotential. Tafel slope, b, is a

DOI: 10.1021/acsami.6b15251
ACS Appl. Mater. Interfaces 2017, 9, 8688−8695

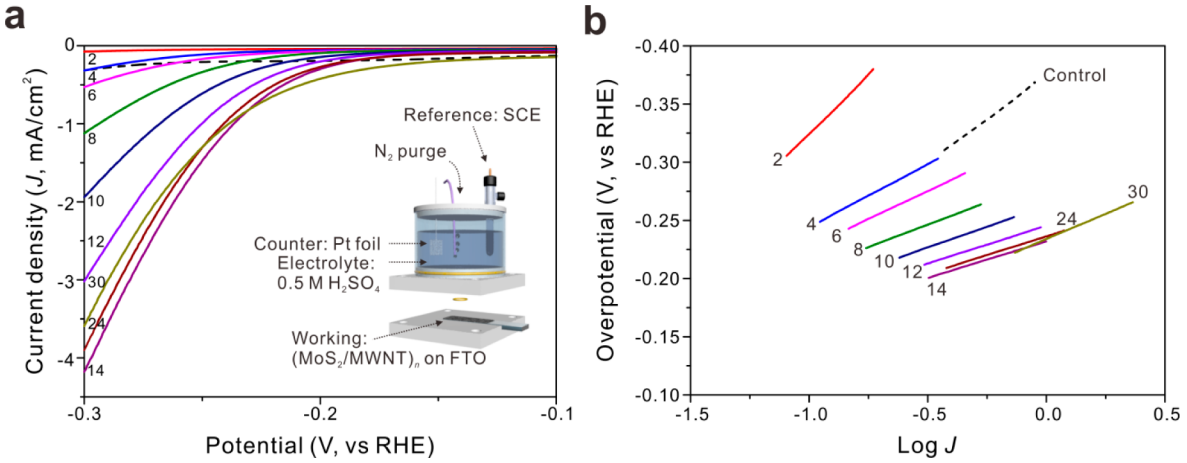

Figure 3. (a) Polarization curves of hybrid multilayer $(MoS_2/MWNT)_n$ electrodes and (b) the corresponding Tafel plot of HER. The curves are labeled by the number of BL (n) in each electrode, and the dotted line is the control sample of a simple mixture. Inset in panel a shows the experimental setup of the three-electrode system. All displayed electrochemical results were after *iR*-correction to account for the Ohmic drops.

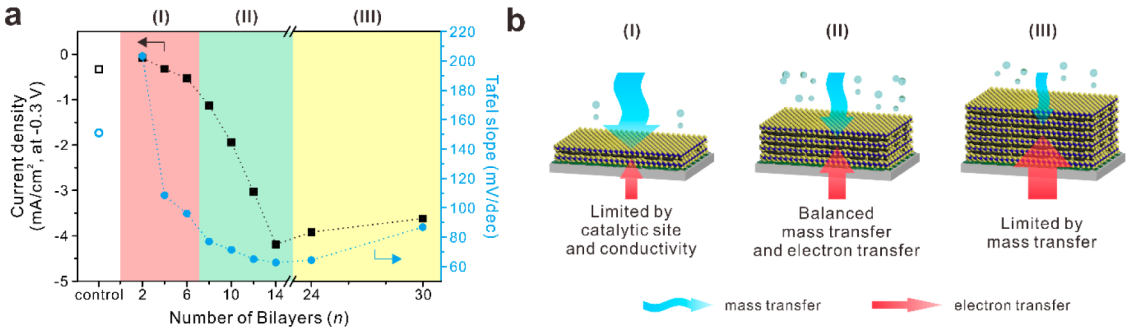

Figure 4. (a) Current density (at −0.3 V, closed square) and Tafel slope (closed circle) of $(MoS_2/MWNT)_n$ multilayers with different number of BL (n). Open square and circle correspond to the control set. (b) Proposed mechanism of the changing electrochemical activity with respect to the film thickness under different electrocatalytic operating regimes.

barometer for the catalytic efficiency of HER and usually determined by the intrinsic properties of the catalyst such as the binding energies to protons and hydrogen molecules. We found that the Tafel slope of $(MoS_2/MWNT)_n$ multilayer film strongly depends on the number of BL (i.e., thickness and architecture of the electrode). For example, b initially decreased with increased number of BL from 200.3 to 62.7 mV/dec between 2 BL and 14 BL and then increased to over 86 mV/dec at 30 BL (Figure 3b). This wide range of Tafel slope (between 62.7−200.3 mV/dec) indicates that the electrocatalytic activity of the thin-film electrode can vary significantly with the film thickness, even when using the identical materials and structure. The optimized Tafel slope of 62.7 mV/dec at 14 BL indicates the better catalytic efficiency than the MoS_2/pyrolytic carbon thin film catalyst[51] and is also comparable to the reported values of other catalysts.[52−54]

The long-term stability of $(MoS_2/MWNT)_{14}$ film toward HER is also assessed by cyclic voltammetry for 200 cycles (Figure S6). Interestingly, its long-term stability was maintained over 200 cycles and even increased slightly (~7%), possibly due to the structural reorganization during the electrochemical cycles and hydrogen evolution.

The trend of the Tafel slope versus BL consists of three regimes, in which different electrocatalytic principles are involved (Figure 4). (I) In the initial stage of assembly (n = 2−6), the Tafel slopes were above 100 mV/dec due to the low amount of catalytic active sites of MoS_2 and insufficient MWNT conductive support, resulting in poor catalytic activity. (II) At moderate thickness (n = 8−14), the increased amounts of catalytic sites and conductive support lead to a good balance between the electron transfer from the electrode and mass transfer from the electrolyte. (III) In thicker films (n = 24−30), excessive loading of the materials could slow the mass transfer into the catalytic film, thus lowering the overall catalytic efficiency of the multilayer film. The same trend was also observed in the current density, onset potential, and overpotential values as a function of BL. The overall electrochemical activity parameters of HER are summarized in Table S1 (see the Supporting Information).

In parallel, we investigated the kinetics of HER with respect to the number of layers by employing electrochemical impedance spectroscopy (EIS). As representative samples, we chose three different $(MoS_2/MWNT)_n$ multilayer electrodes, including thin (4 BL), moderate (14 BL), and thick (24 BL) film electrodes. The Nyquist plots showed that $(MoS_2/MWNT)_{14}$ film with a moderate film thickness displayed the smallest charge transfer resistance (R_{ct}) value of 33.9 Ω than those of thin (4 BL, 1580 Ω) and thicker films (24 BL, 60.9 Ω), indicating the fastest Faradaic process for the optimized hydrogen evolution kinetics (Figure S7). Hence, these results highlighted our claim that the film thickness is critical for thin-film based electrochemical reactions. In a clear contrast, the control set consisting of a simple mixture of the two components showed a considerably lower catalytic activity in

DOI: 10.1021/acsami.6b15251
ACS Appl. Mater. Interfaces 2017, 9, 8688−8695

terms of both current density (−0.32 mA/cm^2) and Tafel slope (173 mV/dec). The poor catalytic activity of the reference electrode is proposed to arise from the randomly distributed catalytic active sites and conductive supporting materials, which form random aggregations that limit the number of exposed electrocatalytically active sites. This comparison suggests the importance of the organized electrode architecture produced with nanoscale precision by LbL assembly, compared to a random composite.

Next, we explored the mechanism of electrocatalytic behavior of the hybrid electrode upon thermal treatment, as the thermal treatment can strongly influence the phase of MoS_2 sheets and the conductivity of the MWNT within the multilayer. We chose the 14 BL multilayer electrode as a representative sample, as it demonstrated the highest catalytic activity among all samples prepared. This electrode was analyzed after annealing for 1 h under three different temperatures (100, 200, and 300 °C; Figure 5). Along with the different temperature conditions, we

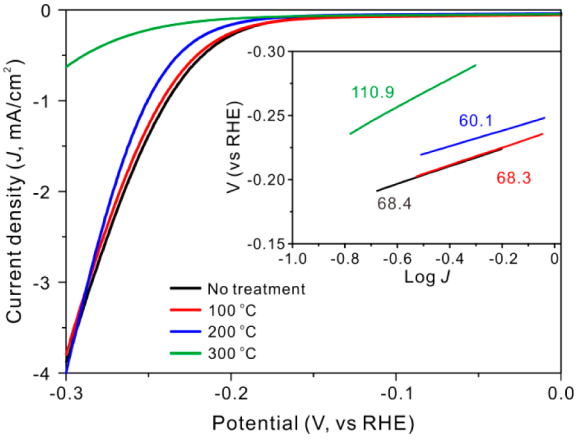

Figure 5. Polarization curves of $(MoS_2/MWNT)_{14}$ multilayer electrodes treated at different annealing temperatures. Inset shows the corresponding Tafel plot from the polarization curve, where the numbers are the corresponding Tafel slopes.

have observed variations in electrochemical behavior such as current density, Tafel slope, and onset potential between the samples. The hybrid electrode annealed at 100 °C did not appear a critical difference in catalytic activities compared to as-prepared $(MoS_2/MWNT)_{14}$. However, the electrode annealed at 200 °C showed the lowest Tafel slope (60.1 mV/dec), indicating the highest electrocatalytic efficiency. The enhanced electrocatalytic activity upon annealing can be attributed to the enhanced electron transfer in MoS_2-based catalysts, as observed in other studies.[9,10] We specifically measured the sheet resistance of $(MoS_2/MWNT)_{14}$, which dramatically decreased from 46.1 kΩ (as-deposited) to 11.4 kΩ (300 °C), due to mild reduction of the MWNT carbon lattices upon removal of surface functional groups (Figure S8).[55] In contrast, the corresponding electrocatalytic activity dropped in the sample treated at 300 °C, as indicated by the significant current drop. It is well-known that thermal treatment promotes the transition from the metastable 1T phase of MoS_2 to the thermodynamically stable 2H phase, and most of MoS_2 is converted to the 2H phase at above 300 °C.[56] Accordingly, the deactivation of catalytic MoS_2 with the increment of annealing temperature was demonstrated by the change in the onset potential and electrochemical surface area (ECSA; Figure S9). For instance, the onset potential for HER gradually shifted from −0.222 to −0.250 V upon annealing at 300 °C. We compared the ECSA of annealed samples by measuring the double-layer capacitance (C_{dl}), as the C_{dl} is proportional to the ECSA. As-deposited $(MoS_2/MWNT)_{14}$ multilayer electrode displayed the highest C_{dl} value (3.09 mF/cm^2) than annealed samples, indicating the decreased electrocatalytic active sites under thermal treatment. In concert with the ECSA measurement, we observed the loss of porous structures as increasing the annealing temperature under SEM (Figure S10).

X-ray photoelectron spectroscopy (XPS) is a powerful tool to provide clear insight into the internal structure and phase of MoS_2. We performed a series of XPS measurements on the $(MoS_2/MWNT)_{14}$ multilayer films to find the relationship between the phase of MoS_2 and the electrochemical properties. For instance, the characteristic peaks of Mo^{4+} $3d_{3/2}$, Mo^{4+} $3d_{5/2}$, and S 2s in MoS_2 were visible at 232.5, 229.3, and 226.2 eV, respectively, regardless of the thermal treatment conditions (Figure 6a). The S 2p spectra can be interpreted in terms of 2H-MoS_2 doublets, with S $2p_{1/2}$ and S $2p_{3/2}$ binding energies of 163.2 and 162.1 eV, respectively. Additionally, the deconvoluted Mo^{4+} $3d_{5/2}$ and S 2p peaks clearly demonstrated the phase transition from 1T to 2H in MoS_2, such that the 1T phase appeared with a binding energy approximately 0.9 eV lower than that of the 2H phase.[57] It was found that the fraction of 1T phase in the entire Mo^{4+} $3d_{5/2}$ peak is 42% before annealing (41% for S $2p_{3/2}$), and disappeared completely at 300 °C (5% for S $2p_{3/2}$). The relatively low content of 1T phase and the appearance Mo^{6+} $3d_{3/2}$ peak at 235.7 eV in every condition may originate from the oxidation of MoS_2 in the aqueous suspension.[58,59] Upon increasing the annealing temperature, the Mo peaks became sharpened with reduced fraction of 1T phase and the associated fwhm (Figure 6b).[56] Taken together, the thermal treatment could enhance the overall electrocatalytic activity of the hybrid multilayer electrocatalyst of $(MoS_2/MWNT)_n$ by optimizing the interplay between the catalytically active MoS_2 and conductive MWNT.

3. CONCLUSION

In summary, we fabricated a hybrid thin film that integrates MoS_2 nanosheets with MWNT and studied the mechanism of the synergistically enhanced catalytic activity toward hydrogen evolution reaction. The electrode was easily fabricated by the LbL assembly of chemically exfoliated few-layered MoS_2 nanosheets with amine-functionalized MWNT, owing to the electrostatic interaction between them. The LbL-assembled electrode showed superior catalytic activity compared to a simple mixture of the two components, demonstrating the importance of nanoscale architecture in these hybrid electrodes. Moreover, the electrocatalytic activity, as characterized by the current density and Tafel slope, was found to strongly depend on the thickness of the multilayer electrode due to the balance between the electron and mass transfers in the system. In addition, thermal treatment at the appropriate temperature further enhanced the catalytic activity through facilitating the electron transfer, while preserving the phase of the electrochemically active MoS_2 nanosheets. We anticipate that the general concept presented in this study will guide the development of hybrid electrodes for next-generation catalysts and energy devices.

DOI: 10.1021/acsami.6b15251
ACS Appl. Mater. Interfaces 2017, 9, 8688−8695

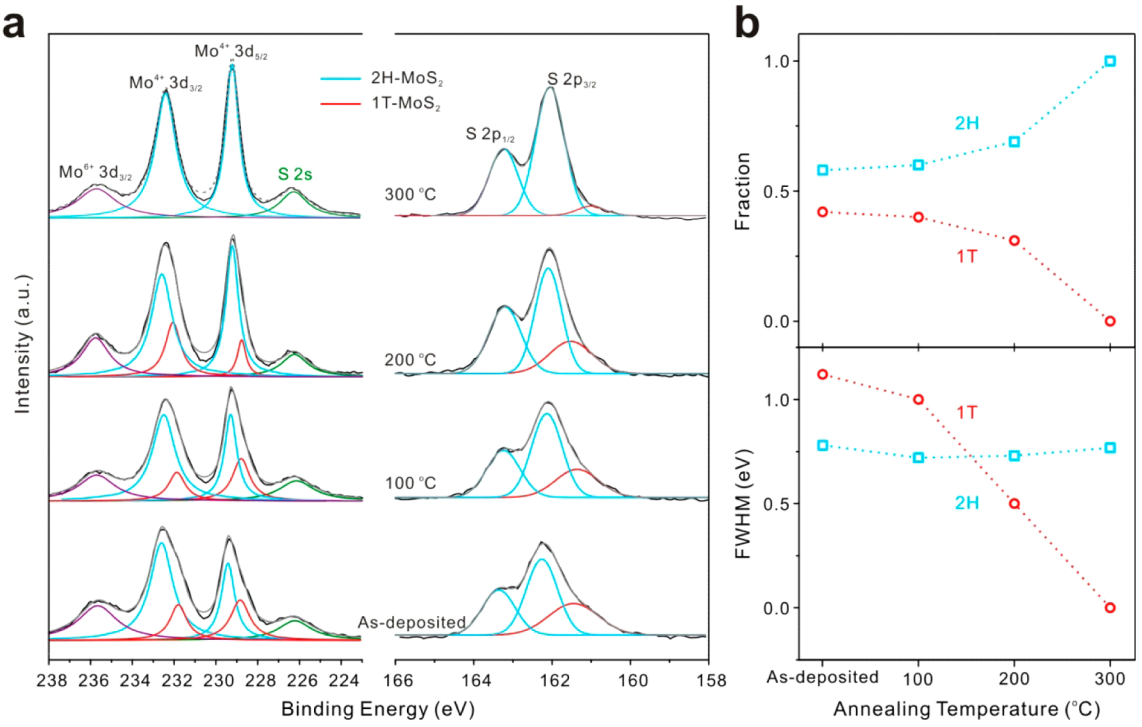

Figure 6. (a) Deconvoluted high-resolution XPS spectra of $(MoS_2/MWNT)_{14}$ multilayer annealed at different temperatures. (b) Areal fraction (top) and fwhm (bottom) of the Mo^{4+} $3d_{5/2}$ peak for the 1T and 2H phases under different annealing temperatures.

■ ASSOCIATED CONTENT

Supporting Information

The Supporting Information is available free of charge on the ACS Publications website at DOI: 10.1021/acsami.6b15251.

Synthetic procedures of the MoS_2 nanosheets and the amine-functionalized MWNT and the process of LbL assembly; additional characterization data using AFM, FT-IR, zeta-potential, Raman, sheet resistance, and electrochemical analyses. (PDF)

■ AUTHOR INFORMATION

Corresponding Author

*E-mail: bskim19@unist.ac.kr.

ORCID

Eungjin Ahn: 0000-0003-2182-7421

Byeong-Su Kim: 0000-0002-6419-3054

Notes

The authors declare no competing financial interest.

■ ACKNOWLEDGMENTS

This work was supported by a National Research Foundation of Korea (NRF) grant (NRF-2014R1A2A1A11052829). E.A. acknowledges financial support from the Global Ph.D. Fellowship funded by National Research Foundation of Korea (NRF-2013H1A2A1033508). We thank Minsu Gu for assistance with QCM analysis and Youngkyu Choi and Yuju Jeon for assistance with FT-IR and SEM, respectively. We would also like to extend our gratitude to Piljae Joo for active discussion on the project.

■ REFERENCES

(1) Vesborg, P. C. K.; Seger, B.; Chorkendorff, I. Recent Development in Hydrogen Evolution Reaction Catalysts and Their Practical Implementation. *J. Phys. Chem. Lett.* **2015**, *6*, 951−957.

(2) Jaramillo, T. F.; Jorgensen, K. P.; Bonde, J.; Nielsen, J. H.; Horch, S.; Chorkendorff, I. Identification of Active Edge Sites for Electrochemical H_2 Evolution from MoS_2 Nanocatalysts. *Science* **2007**, *317*, 100−102.

(3) Zou, X.; Zhang, Y. Noble Metal-Free Hydrogen Evolution Catalysts for Water Splitting. *Chem. Soc. Rev.* **2015**, *44*, 5148−5180.

(4) Bonde, J.; Moses, P. G.; Jaramillo, T. F.; Norskov, J. K.; Chorkendorff, I. Hydrogen Evolution on Nano-Particulate Transition Metal Sulfides. *Faraday Discuss.* **2009**, *140*, 219−231.

(5) Chhowalla, M.; Shin, H. S.; Eda, G.; Li, L.-J.; Loh, K. P.; Zhang, H. The Chemistry of Two-Dimensional Layered Transition Metal Dichalcogenide Nanosheets. *Nat. Chem.* **2013**, *5*, 263−275.

(6) Rowley-Neale, S. J.; Brownson, D. A. C.; Smith, G. C.; Sawtell, D. A. G.; Kelly, P. J.; Banks, C. E. 2D Nanosheet Molybdenum Disulphide (MoS_2) Modified Electrodes Explored towards the Hydrogen Evolution Reaction. *Nanoscale* **2015**, *7*, 18152−18168.

(7) Voiry, D.; Yang, J.; Chhowalla, M. Recent Strategies for Improving the Catalytic Activity of 2D TMD Nanosheets Toward the Hydrogen Evolution Reaction. *Adv. Mater.* **2016**, *28*, 6197−6206.

(8) Tang, Q.; Jiang, D. Mechanism of Hydrogen Evolution Reaction on 1T-MoS_2 from First Principles. *ACS Catal.* **2016**, *6*, 4953−4961.

(9) Cummins, D. R.; Martinez, U.; Sherehiy, A.; Kappera, R.; Martinez-Garcia, A.; Schulze, R. K.; Jasinski, J.; Zhang, J.; Gupta, R. K.; Lou, J.; Chhowalla, M.; Sumanasekera, G.; Mohite, A. D.; Sunkara, M. K.; Gupta, G. Efficient Hydrogen Evolution in Transition Metal Dichalcogenides via a Simple One-Step Hydrazine Reaction. *Nat. Commun.* **2016**, *7*, 11857.

(10) Voiry, D.; Fullon, R.; Yang, J.; de Carvalho Castro e Silva, C.; Kappera, R.; Bozkurt, I.; Kaplan, D.; Lagos, M. J.; Batson, P. E.; Gupta, G.; Mohite, A. D.; Dong, L.; Er, D.; Shenoy, V. B.; Asefa, T.; Chhowalla, M. The Role of Electronic Coupling between Substrate and 2D MoS_2 Nanosheets in Electrocatalytic Production of Hydrogen. *Nat. Mater.* **2016**, *15*, 1003−1009.

DOI: 10.1021/acsami.6b15251
ACS Appl. Mater. Interfaces 2017, 9, 8688−8695

(11) Karunadasa, H. I.; Montalvo, E.; Sun, Y.; Majda, M.; Long, J. R.; Chang, C. J. A Molecular MoS_2 Edge Site Mimic for Catalytic Hydrogen Generation. *Science* **2012**, *335*, 698−702.
(12) Hinnemann, B.; Moses, P. G.; Bonde, J.; Jørgensen, K. P.; Nielsen, J. H.; Horch, S.; Chorkendorff, I.; Nørskov, J. K. Biomimetic Hydrogen Evolution: MoS_2 Nanoparticles as Catalyst for Hydrogen Evolution. *J. Am. Chem. Soc.* **2005**, *127*, 5308−5309.
(13) Li, Y.; Wang, H.; Xie, L.; Liang, Y.; Hong, G.; Dai, H. MoS_2 Nanoparticles Grown on Graphene: An Advanced Catalyst for the Hydrogen Evolution Reaction. *J. Am. Chem. Soc.* **2011**, *133*, 7296−7299.
(14) Kibsgaard, J.; Chen, Z.; Reinecke, B. N.; Jaramillo, T. F. Engineering the Surface Structure of MoS_2 to Preferentially Expose Active Edge Sites for Electrocatalysis. *Nat. Mater.* **2012**, *11*, 963−969.
(15) Liao, L.; Zhu, J.; Bian, X.; Zhu, L.; Scanlon, M. D.; Girault, H. H.; Liu, B. MoS_2 Formed on Mesoporous Graphene as a Highly Active Catalyst for Hydrogen Evolution. *Adv. Funct. Mater.* **2013**, *23*, 5326−5333.
(16) Chen, Z.; Cummins, D.; Reinecke, B. N.; Clark, E.; Sunkara, M. K.; Jaramillo, T. F. Core−shell MoO_3−MoS_2 Nanowires for Hydrogen Evolution: A Functional Design for Electrocatalytic Materials. *Nano Lett.* **2011**, *11*, 4168−4175.
(17) Cummins, D. R.; Martinez, U.; Kappera, R.; Voiry, D.; Martinez-Garcia, A.; Jasinski, J.; Kelly, D.; Chhowalla, M.; Mohite, A. D.; Sunkara, M. K.; Gupta, G. Catalytic Activity in Lithium-Treated Core−Shell MoO_x/MoS_2 Nanowires. *J. Phys. Chem. C* **2015**, *119*, 22908−22914.
(18) Tao, L.; Duan, X.; Wang, C.; Duan, X.; Wang, S. Plasma-Engineered MoS_2 Thin-Film as an Efficient Electrocatalyst for Hydrogen Evolution Reaction. *Chem. Commun.* **2015**, *51*, 7470−7473.
(19) Shin, S.; Jin, Z.; Kwon, D. H.; Bose, R.; Min, Y.-S. High Turnover Frequency of Hydrogen Evolution Reaction on Amorphous MoS_2 Thin Film Directly Grown by Atomic Layer Deposition. *Langmuir* **2015**, *31*, 1196−1202.
(20) McAteer, D.; Gholamvand, Z.; McEvoy, N.; Harvey, A.; O'Malley, E.; Duesberg, G. S.; Coleman, J. N. Thickness Dependence and Percolation Scaling of Hydrogen Production Rate in MoS_2 Nanosheet and Nanosheet−Carbon Nanotube Composite Catalytic Electrodes. *ACS Nano* **2016**, *10*, 672−683.
(21) Lvov, Y.; Ariga, K.; Ichinose, I.; Kunitake, T. Assembly of Multicomponent Protein Films by Means of Electrostatic Layer-by-Layer Adsorption. *J. Am. Chem. Soc.* **1995**, *117*, 6117−6123.
(22) Decher, G. Fuzzy Nanoassemblies: Toward Layered Polymeric Multicomposites. *Science* **1997**, *277*, 1232−1237.
(23) Lvov, Y.; Ariga, K.; Onda, M.; Ichinose, I.; Kunitake, T. A Careful Examination of the Adsorption Step in the Alternate Layer-by-Layer Assembly of Linear Polyanion and Polycation. *Colloids Surf., A* **1999**, *146*, 337−346.
(24) Hammond, P. T. Form and Function in Multilayer Assembly: New Applications at the Nanoscale. *Adv. Mater.* **2004**, *16*, 1271−1293.
(25) Jiang, C.; Markutsya, S.; Tsukruk, V. V. Compliant, Robust, and Truly Nanoscale Free-Standing Multilayer Films Fabricated Using Spin-Assisted Layer-by-Layer Assembly. *Adv. Mater.* **2004**, *16*, 157−161.
(26) Podsiadlo, P.; Michel, M.; Lee, J.; Verploegen, E.; Wong Shi Kam, N.; Ball, V.; Lee, J.; Qi, Y.; Hart, A. J.; Hammond, P. T.; Kotov, N. A. Exponential Growth of LBL Films with Incorporated Inorganic Sheets. *Nano Lett.* **2008**, *8*, 1762−1770.
(27) Hong, J.; Han, J. Y.; Yoon, H.; Joo, P.; Lee, T.; Seo, E.; Char, K.; Kim, B.-S. Carbon-Based Layer-by-Layer Nanostructures: From Films to Hollow Capsules. *Nanoscale* **2011**, *3*, 4515−4531.
(28) Ariga, K.; Yamauchi, Y.; Rydzek, G.; Ji, Q.; Yonamine, Y.; Kevin, C.-W.; Hill, J. P. Layer-by-Layer Nanoarchitectonics: Invention, Innovation, and Evolution. *Chem. Lett.* **2014**, *43*, 36−68.
(29) Richardson, J. J.; Bjornmalm, M.; Caruso, F. Technology-Driven Layer-by-Layer Assembly of Nanofilms. *Science* **2015**, *348*, 411.
(30) Lee, T.; Min, S. H.; Gu, M.; Jung, Y. K.; Lee, W.; Lee, J. U.; Seong, D. G.; Kim, B. Layer-by-Layer Assembly for Graphene-Based Multilayer Nanocomposites: Synthesis and Applications. *Chem. Mater.* **2015**, *27*, 3785−3796.
(31) Ahn, E.; Lee, T.; Gu, M.; Park, M.; Min, S. H.; Kim, B.-S. Layer-by-Layer Assembly for Graphene-Based Multilayer Nanocomposites: The Field Manual. *Chem. Mater.* **2017**, *29*, 69−79.
(32) Kotov, N. A.; Dékány, I.; Fendler, J. H. Ultrathin Graphite Oxide-Polyelectrolyte Composites Prepared by Self-Assembly: Transition between Conductive and Non-Conductive States. *Adv. Mater.* **1996**, *8*, 637−641.
(33) Hong, T.-K.; Lee, D. W.; Choi, H. J.; Shin, H. S.; Kim, B.-S. Transparent, Flexible Conducting Hybrid Multilayer Thin Films of Multiwalled Carbon Nanotubes with Graphene Nanosheets. *ACS Nano* **2010**, *4*, 3861−3868.
(34) Kulkarni, D. D.; Choi, I.; Singamaneni, S. S.; Tsukruk, V. V. Graphene Oxide−Polyelectrolyte Nanomembranes. *ACS Nano* **2010**, *4*, 4667−4676.
(35) Zhu, J.; Shim, B. S.; Di Prima, M.; Kotov, N. A. Transparent Conductors from Carbon Nanotubes LBL-Assembled with Polymer Dopant with $\pi-\pi$ Electron Transfer. *J. Am. Chem. Soc.* **2011**, *133*, 7450−7460.
(36) Lee, D. W.; Hong, T.-K.; Kang, D.; Lee, J.; Heo, M.; Kim, J. Y.; Kim, B.-S.; Shin, H. S. Highly Controllable Transparent and Conducting Thin Films Using Layer-by-Layer Assembly of Oppositely Charged Reduced Graphene Oxides. *J. Mater. Chem.* **2011**, *21*, 3438−3442.
(37) Zhu, J.; Zhang, H.; Kotov, N. A. Thermodynamic and Structural Insights into Nanocomposites Engineering by Comparing Two Materials Assembly Techniques for Graphene. *ACS Nano* **2013**, *7*, 4818−4829.
(38) Joo, P.; Jo, K.; Ahn, G.; Voiry, D.; Jeong, H. Y.; Ryu, S.; Chhowalla, M.; Kim, B.-S. Functional Polyelectrolyte Nanospaced MoS_2 Multilayers for Enhanced Photoluminescence. *Nano Lett.* **2014**, *14*, 6456−6462.
(39) Shen, J.; Pei, Y.; Dong, P.; Ji, J.; Cui, Z.; Yuan, J.; Baines, R.; Ajayan, P. M.; Ye, M. Layer-by-Layer Self-Assembly of Polyelectrolyte Functionalized MoS_2 Nanosheets. *Nanoscale* **2016**, *8*, 9641−9647.
(40) Chang, Y.-H.; Nikam, R. D.; Lin, C.-T.; Huang, J.-K.; Tseng, C.-C.; Hsu, C.-L.; Cheng, C.-C.; Su, C.-Y.; Li, L.-J.; Chua, D. H. C. Enhanced Electrocatalytic Activity of MoS_x on TCNQ-Treated Electrode for Hydrogen Evolution Reaction. *ACS Appl. Mater. Interfaces* **2014**, *6*, 17679−17685.
(41) Yu, X.-Y.; Hu, H.; Wang, Y.; Chen, H.; Lou, X. W. D. Ultrathin MoS_2 Nanosheets Supported on N-Doped Carbon Nanoboxes with Enhanced Lithium Storage and Electrocatalytic Properties. *Angew. Chem., Int. Ed.* **2015**, *54*, 7395−7398.
(42) Yu, X.-Y.; Feng, Y.; Jeon, Y.; Guan, B.; Lou, X. W. D.; Paik, U. Formation of Ni−Co−MoS_2 Nanoboxes with Enhanced Electrocatalytic Activity for Hydrogen Evolution. *Adv. Mater.* **2016**, *28*, 9006−9011.
(43) Yang, L.; Zhou, W.; Lu, J.; Hou, D.; Ke, Y.; Li, G.; Tang, Z.; Kang, X.; Chen, S. Hierarchical Spheres Constructed by Defect-Rich MoS_2/carbon Nanosheets for Efficient Electrocatalytic Hydrogen Evolution. *Nano Energy* **2016**, *22*, 490−498.
(44) Li, D. J.; Maiti, U. N.; Lim, J.; Choi, D. S.; Lee, W. J.; Oh, Y.; Lee, G. Y.; Kim, S. O. Molybdenum Sulfide/N-Doped CNT Forest Hybrid Catalysts for High-Performance Hydrogen Evolution Reaction. *Nano Lett.* **2014**, *14*, 1228−1233.
(45) Ekspong, J.; Sharifi, T.; Shchukarev, A.; Klechikov, A.; Wågberg, T.; Gracia-Espino, E. Stabilizing Active Edge Sites in Semicrystalline Molybdenum Sulfide by Anchorage on Nitrogen-Doped Carbon Nanotubes for Hydrogen Evolution Reaction. *Adv. Funct. Mater.* **2016**, *26*, 6766−6776.
(46) Heising, J.; Kanatzidis, M. G. Exfoliated and Restacked MoS_2 and WS_2: Ionic or Neutral Species? Encapsulation and Ordering of Hard Electropositive Cations. *J. Am. Chem. Soc.* **1999**, *121*, 11720−11732.
(47) Lee, S. W.; Kim, B.-S.; Chen, S.; Shao-Horn, Y.; Hammond, P. T. Layer-by-Layer Assembly of All Carbon Nanotube Ultrathin Films

DOI: 10.1021/acsami.6b15251
ACS Appl. Mater. Interfaces 2017, 9, 8688−8695

for Electrochemical Applications. *J. Am. Chem. Soc.* **2009**, *131*, 671−679.
(48) Singh, B. P.; Singh, D.; Mathur, R. B.; Dhami, T. L. Influence of Surface Modified MWCNTs on the Mechanical, Electrical and Thermal Properties of Polyimide Nanocomposites. *Nanoscale Res. Lett.* **2008**, *3*, 444−453.
(49) Silva, W. M.; Ribeiro, H.; Seara, L. M.; Calado, H. D. R.; Ferlauto, A. S.; Paniago, R. M.; Leite, C. F.; Silva, G. G. Surface Properties of Oxidized and Aminated Multi-Walled Carbon Nanotubes. *J. Braz. Chem. Soc.* **2012**, *23*, 1078−1086.
(50) Odedairo, T.; Ma, J.; Gu, Y.; Chen, J.; Zhao, X. S.; Zhu, Z. One-Pot Synthesis of Carbon Nanotube-Graphene Hybrids via Syngas Production. *J. Mater. Chem. A* **2014**, *2*, 1418−1428.
(51) Nolan, H.; McEvoy, N.; O'Brien, M.; Berner, N. C.; Yim, C.; Hallam, T.; McDonald, A. R.; Duesberg, G. S. Molybdenum Disulfide/pyrolytic Carbon Hybrid Electrodes for Scalable Hydrogen Evolution. *Nanoscale* **2014**, *6*, 8185−8191.
(52) Wu, Z.; Fang, B.; Wang, Z.; Wang, C.; Liu, Z.; Liu, F.; Wang, W.; Alfantazi, A.; Wang, D.; Wilkinson, D. P. MoS_2 Nanosheets: A Designed Structure with High Active Site Density for the Hydrogen Evolution Reaction. *ACS Catal.* **2013**, *3*, 2101−2107.
(53) Wang, H.; Lu, Z.; Kong, D.; Sun, J.; Hymel, T. M.; Cui, Y. Electrochemical Tuning of MoS_2 Nanoparticles on Three-Dimensional Substrate for Efficient Hydrogen Evolution. *ACS Nano* **2014**, *8*, 4940−4947.
(54) Benson, J.; Li, M.; Wang, S.; Wang, P.; Papakonstantinou, P. Electrocatalytic Hydrogen Evolution Reaction on Edges of a Few Layer Molybdenum Disulfide Nanodots. *ACS Appl. Mater. Interfaces* **2015**, *7*, 14113−14122.
(55) Pei, S.; Cheng, H.-M. The Reduction of Graphene Oxide. *Carbon* **2012**, *50*, 3210−3228.
(56) Eda, G.; Yamaguchi, H.; Voiry, D.; Fujita, T.; Chen, M.; Chhowalla, M. Photoluminescence from Chemically Exfoliated MoS_2. *Nano Lett.* **2011**, *11*, 5111−5116.
(57) Acerce, M.; Voiry, D.; Chhowalla, M. Metallic 1T Phase MoS_2 Nanosheets as Supercapacitor Electrode Materials. *Nat. Nanotechnol.* **2015**, *10*, 313−318.
(58) Weber, T.; Muijsers, J. C.; van Wolput, J. H. M. C.; Verhagen, C. P. J.; Niemantsverdriet, J. W. Basic Reaction Steps in the Sulfidation of Crystalline MoO_3 to MoS_2, As Studied by X-Ray Photoelectron and Infrared Emission Spectroscopy. *J. Phys. Chem.* **1996**, *100*, 14144−14150.
(59) Su, S.-H.; Hsu, W.-T.; Hsu, C.-L.; Chen, C.-H.; Chiu, M.-H.; Lin, Y.-C.; Chang, W.-H.; Suenaga, K.; He, J.-H.; Li, L.-J. Controllable Synthesis of Band-Gap-Tunable and Monolayer Transition-Metal Dichalcogenide Alloys. *Front. Energy Res.* **2014**, *2*, 27.

DOI: 10.1021/acsami.6b15251
ACS Appl. Mater. Interfaces 2017, 9, 8688−8695